

1 Spectral shortcut in turbulence energy transfer in open channel flow over
2 submerged vegetation

3

4 Hanqing Zhao^{1,2}, Hongwu Tang^{1,3,‡}, Jing Yan¹, Dongfang Liang⁴, Jinyu Zheng⁵

5 ¹ *State Key Laboratory of Hydrology-Water Resources and Hydraulic Engineering, Hohai University,*
6 *Nanjing, China*

7 ² *China Three Gorges Corporation, Beijing, China*

8 ³ *Yangtze Institute for Conservation & Development, Nanjing, China*

9 ⁴ *Department of Engineering, University of Cambridge, Cambridge, UK*

10 ⁵ *Henan Water Conservancy Survey, Ltd., Zhengzhou, China*

11 [‡] Corresponding author: Hongwu Tang, hwtang@hhu.edu.cn

12

1 **Abstract**

2 This study explores the characteristics of the spectral shortcut in the turbulence kinetic energy transfer
3 in experimental open channel flows with the presence of submerged vegetation flow. The vegetation
4 layer was simulated by arrays of rigid vertical cylinders, distributed uniformly in the channel bed.
5 Results indicate that there are dual inertial subranges (ISRs) in the spectral distribution of turbulence
6 energy in the penetration layer, where the Kelvin-Helmholtz (KH) and wake vortices coexist. The
7 lower-frequency and higher-frequency ISRs reflect the energy cascading of the KH and wake-scale
8 vortices, respectively. Spectral shortcut narrows the ISR for the KH vortex and contributes to the ISR
9 for the wake-scale vortices, because such an action transfers a significant amount of turbulent energy
10 directly from the large-scale eddies to the wake-scale vortices. We study the influence of spectral
11 shortcut on energy transfer according to the turbulence kinetic energy budget equation for shear
12 turbulence. The transferred energy is found to account for 58-71% of the shear turbulent energy and
13 contributes considerably to the wake-scale turbulence. The strength of the energy transfer increases
14 with the increase in the vegetation density and the mean bulk velocity and the decrease in the relative
15 submergence.

16 **Key words:** spectral shortcut; dual inertial subranges; penetration layer; energy transfer; wake-scale
17 turbulence

1 **1. Introduction**

2 Aquatic vegetation is an important component of river ecosystems that can promote biodiversity
3 by enhancing the spatial heterogeneity in flow conditions and habitats (Kemp et al., 2000; Liu et al.,
4 2010; Choi and Kang, 2016). Canopy flow also affects the incipient motion, transport and deposition
5 of sediment, resulting in changes in the distribution of sediment grain size (Yang & Choi, 2010; Nepf,
6 2012a), bed slope (Bouteiller & Venditti, 2014) and channel morphology (Bouteiller & Venditti, 2015;
7 Perignon et al., 2013). Research into the dynamics of the vegetated flow can help better understand
8 the river ecology and channel geomorphology.

9 Generally speaking, there are two types of vortices in open channel flows through submerged
10 vegetation. These are the low frequency Kelvin-Helmholtz (KH) vortex driven by the KH instability
11 in the longitudinal-vertical (x - z) plane within the mixing layer ($h_p < z < h_o$ in Fig. 1), and the high
12 frequency wake vortex generated by individual plants in the longitudinal-lateral (x - y) plane within
13 canopy ($0 < z < h_v$ in Fig. 1) (Zong & Nepf, 2010; Nepf & Ghisalberti, 2008). Here h_p and h_o are the
14 lower and upper boundaries that are characterized with turbulent kinetic energy (TKE) balance
15 between the shear turbulence generation and dissipation terms (Wilson, 1988), and h_v is the
16 submerged vegetation height. As part of the KH vortex penetrates the canopy, with the penetration
17 layer located at $h_p < z < h_v$ in Fig.1, the vegetation breaks it into several secondary, small-scale vortices
18 (Hout et al. 2007). This KH vortex break-up mechanism interferes the eddy cascading process, and
19 this phenomenon is defined as the “spectral shortcut” (Finnigan, 2000).

20 Spectral shortcut affects the turbulent coherent structure and the flow characteristics over the
21 whole depth. This action directly transfers the TKE from large-scale turbulence to the small-scale
22 turbulence (Finnigan, 2000), thereby weakening the dominance of the KH vortex in the mixing layer.
23 An analytical formula has been established to evaluate TKE transfer rate over the terrestrial canopy,
24 where the air flow is laterally unconfined (Wilson, 1988). The influence of the spectral shortcut on
25 the eddy distribution can be investigated by examining the turbulence spectra. According to the
26 vertical velocity spectra in submerged vegetated flow, the spectrum peaks at a frequency
27 corresponding to the generated secondary vortices; and the scales of the secondary vortices are same
28 as those of the wake vortices (Poggi et al., 2004; King et al., 2012). The aggregation of the secondary

1 vortex and the wake vortex is defined as the “wake-scale vortex”. Since the KH, secondary and wake
 2 vortices co-exist in longitudinal direction, the longitudinal velocity spectra reflect the interaction of
 3 all the turbulent structures. Meanwhile, the TKE dissipation and vertical flow subdivision can also be
 4 reflected according to the longitudinal velocity spectra (Nezu & Sanjou, 2008; Nepf & Vivoni, 2000).
 5 However, detailed studies about the longitudinal velocity spectra have been rarely conducted
 6 previously.

7 This study investigates various aspects of the spectral shortcut by analyzing the longitudinal
 8 velocity spectra based on the measurements in an experimental flume. The main goal is to explore
 9 the influences of the spectral shortcut on the turbulence structure and energy transfer mechanism by
 10 making use of the spectral and TKE budget analyses, respectively. The Results & Discussion Section
 11 is the main part of this article and is structured as follows. In Section 4.1, the energy cascading
 12 processes for the shear and wake vortices are separately investigated by analyzing the turbulent
 13 spectra above and below the mixing layer, i.e., in the outer zone with $h_o < z < H$ and the lower canopy
 14 zone with $0 < z < h_p$ (see Fig. 1). In Section 4.2, the longitudinal velocity spectra in the penetration
 15 layer are analyzed. Section 4.3 studies the flow subdivision based on TKE balance and Section 4.4
 16 estimates the energy transfer by examining the TKE budget. The various influencing factors of the
 17 spectral shortcut are explored according to the TKE transfer rate, which can be revealed by combining
 18 the TKE budget and flow subdivision results together.

19 **2. Turbulent Kinetic Energy Budget Equation**

20 The turbulent kinetic energy (TKE) budget equation is introduced here as the fundamental
 21 backdrop, because both flow subdivision and energy transfer are studied by making use of this
 22 equation. A horizontal plane-averaging procedure has been commonly conducted to study the
 23 submerged vegetation flow in an open channel (Nepf, 2012b; Nezu & Sanjou, 2008; Nepf & Vivoni,
 24 2000). The temporal and horizontal averaged TKE conservation equation is presented below, with
 25 some less important terms being omitted (Nezu & Sanjou, 2008; Finnigan, 2000; Nepf et al., 2007;
 26 Raupach & Shaw, 1982).

$$27 \quad \frac{\partial \langle \bar{k} \rangle}{\partial t} = \langle -\overline{uw} \rangle \frac{\partial \langle U \rangle}{\partial z} + \left\langle -\overline{u_i u_j} \frac{\partial U_i''}{\partial x_j} \right\rangle + \frac{\partial}{\partial z} \langle -\bar{k} \cdot w \rangle + \frac{\partial}{\partial z} \langle -\bar{k}'' \cdot W'' \rangle + \frac{\partial}{\partial z} \left\langle \frac{\overline{p}}{\rho} \cdot w \right\rangle + \nu \frac{\partial^2}{\partial z^2} \langle \bar{k} \rangle - \langle \varepsilon \rangle \quad (1)$$

1 where i and j are indices running from 1 to 3, x_j stands for three Cartesian spatial directions, the time
2 averaging operator is denoted by an over bar, the horizontal space average one is denoted by the
3 brackets and a double prime is applied to represent the deviation from the space- and time- averaged
4 value, U is the time-averaged streamwise velocity, W is the time- averaged vertical velocity, u , v and
5 w denote the velocity fluctuations, and u' , v' and w' denote the r. m. s. values, i.e., $u' = \sqrt{\frac{1}{N} \sum_{i=1}^N (u^2)}$,
6 $v' = \sqrt{\frac{1}{N} \sum_{i=1}^N (v^2)}$, and $w' = \sqrt{\frac{1}{N} \sum_{i=1}^N (w^2)}$, and N is the total sample number, $k = (u^2+v^2+w^2)/2$ is the
7 instantaneous TKE per unit mass, $-\overline{uw}$ is the time-mean value of the turbulent shear stress,
8 $\overline{uw} = \frac{1}{N} \sum_{i=1}^N (u \cdot w)$.

9 The third, fourth, fifth, sixth and seventh terms on the right hand of Eq. (1) represent the turbulent
10 transport rate, the dispersive transport rate, the pressure diffusion rate, the viscous diffusion rate, and
11 the viscous dissipation rate, respectively. The first and second terms on the right hand of Eq. (1) are
12 defined as G_S and G_W , and they represent TKE generation rates due to the shear and wake turbulence,
13 respectively (Nepf, 2012b). G_W is distributed throughout the canopy layer, and it can be calculated
14 approximately by the product of canopy form-drag and the flow velocity (Nepf & Vivoni, 2000; Nezu
15 & Sanjou, 2008).

$$16 \quad G_W = \frac{1}{2} C_d \frac{\lambda}{h_v} \langle U \rangle^3 \quad (2)$$

17 where C_d is the local element drag coefficient provided by Tang et al. (2014).

18 The TKE dissipation rate ε can be evaluated by looking at the spectra for the frequencies within
19 the inertial subrange (ISR) where the Kolmogorov's -5/3 power law is satisfied (Ricardo et al., 2014;
20 Nepf & Vivoni, 2000). Thus, the following formula has been proposed,

$$21 \quad F(f) = 0.5 \cdot \varepsilon^{2/3} \cdot f^{-1} \cdot (2\pi f / U_c)^{-2/3} \quad (3)$$

22 where f is the frequency of velocity fluctuation, $F(f)$ is the spectral density, and U_c is the convective
23 velocity of mean eddies (Nezu & Sanjou, 2008). U_c increases with flow speed U (Mandel et al., 2017),
24 and the ratio U_c/U has been set to a constant of 1 or 2 in order to calculate ε in the previous studies
25 (Chen, 2016; Liu et al., 2001; Nezu et al., 2006). In this study, the U_c/U ratio is set to be 1.5 in
26 accordance with the U_c and U profiles presented in Nezu and Sanjou (2008).

1 For the case of steady uniform and turbulent flow, $\partial \langle \bar{k} \rangle / \partial t$, the dispersive transport rate and the
2 viscous diffusion rate are nearly zero (Nezu & Sanjou, 2008). Therefore, Eq. (1) is rearranged to be:

$$3 \quad G_s + G_w + T - \langle \varepsilon \rangle = 0 \quad (4)$$

4 where T represents the TKE transport along the z direction and is a sum of the turbulent transport rate
5 and the pressure diffusion rate.

6 **3. Experimental Set-up and Measurement**

7 Experiments were conducted in a glass-walled recirculating flume of 12 m in length, 0.6 m in
8 width ($B = 0.6\text{m}$) and 0.6 m in depth in the Sediment Research Laboratory at Hohai University (Fig.
9 2). The flow discharge Q was controlled by the variable frequency pump and flow meter system at
10 the flume inlet with an accuracy of 0.001 L s^{-1} , and the flow depth H was controlled by the tailgate at
11 the outlet with an accuracy of 0.5 mm. The flume bed slope S was adjustable to maintain a constant
12 water depth in the canopy region. The combined adjustment of the pump, tailgate and the bed slope
13 created a steady and uniform flow condition, in which Q and H values obtain desired values.

14 An array of circular aluminum cylinders (diameter $d_v = 0.6 \text{ cm}$ and height $h_v = 6 \text{ cm}$) were used
15 to simulate the rigid canopy model, which covered the bed area of 8 m long and 0.6 m wide at the
16 mid length of the flume. The longitudinal and lateral distances between neighboring vegetation
17 elements were set as S_x and S_y , respectively. The frontal vegetation area per unit bed area was set as
18 $\lambda = d_v h_v / (S_x \cdot S_y)$.

19 The 3D flow velocity was measured by acoustic Doppler velocimeters (ADV, Nortek, Norway)
20 with an accuracy of $\pm 1 \text{ mm s}^{-1}$. Velocity profiles were measured 5 m downstream of the leading edge
21 of the canopy section, where the flow was fully developed in the longitudinal direction (Nepf &
22 Ghisalberti, 2008; Okamoto & Nezu, 2013). Flow velocities at two locations (locations 1 & 2 in Fig.
23 2) in the test area were measured and averaged to represent the canopy flow. Locations 1 and 2 were
24 laterally separated, one lying in the cylinder's wake region and the other in the free stream (Fig. 2).
25 The arrangement of gauging points was similar to that in Huai et al. (2009) and Tang et al. (2014),
26 and the rationality of overall flow measurement has been validate by Zhao et al. (2019). The sampling
27 duration was set to be 180 seconds with a frequency of 200 Hz. The measured raw data were processed
28 by removing weak signals (<10% signal-to-noise ratio), poor correlated signals (<70% correlation),

1 and despiking (Yuan et al., 2016).

2 Table 1 shows the experimental conditions, where H/h_v is the relative degree of submergence,
3 and U_m is the mean bulk velocity with $U_m = Q/(BH)$. The stem density, the relative submergence and
4 the mean flow velocity were varied in the experiments. Vegetation density λ was set to be larger than
5 0.1 in this study to make sure that the KH instability occurred in each of the cases (Nepf, 2012a). The
6 vegetation height h_v was maintained constant in each cases, and the submergence H/h_v was adjusted
7 by changing the flow depth H . The values of H/h_v ranged from 2 to 7, corresponding to a change from
8 the depth-limited flow to the shallowly-submerged flow. U_m was set to 20 or 30 cm s⁻¹ so that drag
9 coefficient of the stems C_d could be adopted from our previous studies (Tang et al., 2014).

10 4. Results and Discussion

11 4.1 Spectra of the shear and wake turbulence

12 The turbulence spectrum presents the occurrence possibility $F(f)$ (i.e., the spectral density) of
13 eddies with varying frequencies f at a fixed point in the turbulent flow. Figure 3 presents spectral
14 distributions in the upper mixing layer (Figs. 3a & 3c) and lower canopy zone (Figs. 3b & 3d) at
15 locations 1 & 2 in Case B-3-30. For turbulence in the upper mixing layer, the spectral density in Fig.
16 3a is larger than that in Fig. 3c, because the KH instability is much fiercer at location 1. [The](#)
17 [corresponding length scales could be determined by flow velocity at the canopy top divided by the](#)
18 [velocity gradient there \(Raupach et al., 1996\)](#), and they were 4.54 cm at location 1 and 2.97 cm at
19 location 2. For flow in lower canopy zone, the spectral density at location 1 (Fig. 3b) is smaller than
20 that at location 2 (Fig. 3d), because location 1 is behind the vegetation element where the water
21 movement is relatively weak. The velocity $U = 8.5$ cm s⁻¹ at location 1 and 10 cm s⁻¹ at location 2.

22 As to the turbulence in the mixing layer, the $F(f)$ attains its maximum at some specific low
23 frequency f , which is regarded as the KH vortex frequency f_{KH} (Ghisalberti & Nepf, 2002). The f_{KH}
24 value dose not vary spatially (Zhao et al., 2019). We thus speculate that the f_{KH} was about 0.15 Hz in
25 Case B-3-30 (Figs. 3a & 3c). The similar feature about the f_{KH} value was also noticed in the work of
26 Wallace et al. (1998).

27 The wake turbulence dominates in lower canopy zone. For the flow passing by a single cylinder,

1 with $d_v = 0.6$ cm and $U = 8.5$ or 10 cm s⁻¹, the shedding frequency of the wake vortex f_{wake} was
2 estimated to be 3 or 3.5 Hz (Blevins, 2006). $F(f)$ attains a peak at these f_{wake} values (Chen & Guo,
3 2013). However, for the flow passing by vegetation arrays, the $F(f)$ shows a spectral plateau, rather
4 than any clear peaks at the f_{wake} (Figs 3b & 3d). The spectral plateau occurs because the wake vortex
5 shedding is being affected by the proximity of the neighboring cylinders (Nepf, 1999; Chen, 2011).
6 The small values of S_x and S_y cause the shedding frequency to vary within a small range lying around
7 the f_{wake} (Fig. 3b, d). In this article, we therefore set the plateau frequency (f_p) as the shedding
8 frequency of wake vortices for vegetation arrays.

9 The inertial subrange (ISR) reflects the process of vortex cascading evolution (Nezu &
10 Nakagawa, 1993; Finnigan, 2000). The ISR values in this investigation were found from the
11 frequency range where $F(f)$ is proportional to $f^{-5/3}$ (i.e., $F(f) \propto f^{-5/3}$). Figure 3 shows that ISR
12 frequencies associated with the KH vortex (ISR_{KH}) and the wake vortex (ISR_p) lie around the values
13 of 10^0 (the shaded region in Figs 3a and 3c) and 10^1 Hz (the shaded region in Figs 3b and 3d),
14 respectively. These ISR frequencies are in line with the findings of Poggi et al. (2004) and Nepf
15 (1999), and they are smaller than the corresponding threshold f_{KH} and f_p values. It may be noted that
16 at the gauging location, where the spectral distribution is plotted (Fig. 3), a single ISR exists either in
17 the lower or in the higher frequency range. This can be attributed to the sole influence of the KH
18 vortex or the wake vortex in these locations.

19 **4. 2 Dual ISRs for turbulent spectra in the penetration layer**

20 Spectral shortcut affects the shear turbulence spectra $F_{\text{KH}}(f)$ in the penetration layer. Figure 4 is
21 a schematic diagram to illustrate this physical process. Eddies of all scales larger than the vegetation
22 stems (i.e., eddies with f values less than f_p) transfer their TKE to the wake-scale turbulence,
23 bypassing the normal energy cascade (Hout et al. 2007; Poggi et al., 2004). This action decreases the
24 $F_{\text{KH}}(f)$ value when $f < f_p$ and increases it when $f \geq f_p$, transforming the turbulence spectrum curve
25 from the solid black line to the dashed black line in Fig. 4. The f_p value lies at the high wavenumber
26 end of the ISR_{KH} (Finnigan, 2000), as shown in Fig. 4. Therefore, the ISR_{KH} , where the Kolmogorov's
27 $-5/3$ power law is satisfied, is narrowed. Meanwhile, the transferred TKE would be dissipated in a
28 way similar to the wake TKE cascade (Wilson, 1988). Spectral shortcut thus leads to the existence of

1 a high frequency range where $F_{KH}(f) \propto f^{-5/3}$ satisfies, as labelled by the black dashed line in Fig. 4.
 2 This frequency range coincides with the ISR_P for the wake turbulence spectra $F_P(f)$, labelled by the
 3 blue dotted line in Fig. 4.

4 As the flow in the penetration layer is affected both by the shear and wake turbulence, the
 5 statistical value of $F(f)$, labelled as the yellow dashed line in Fig. 4, represents a sum of $F_{KH}(f)$ and
 6 $F_P(f)$.

7 Figure 5 presents the turbulent spectra $F(f)$ in the penetration layer in this study. Turbulence
 8 with dual ISRs has been reported in studies of river, atmospheric and ocean dynamics because of the
 9 coexistence of different flow structures, which are characterized with significantly different length
 10 scales (Monin & Yaglom, 1975; Nezu & Nakagawa, 1993). However, the phenomenon of dual ISRs
 11 for the canopy flow has not been reported before. This is, perhaps, because previous studies only
 12 analyzed the spectral distribution at a low frequency range from 10^{-3} to 10^0 Hz (Ghisalberti & Nepf,
 13 2002, 2006), while the high- frequency ISR could not be observed in their measurement system.

14 This article investigates the dual ISRs phenomenon by analyzing the shear and wake turbulence
 15 in a combined manner. Here, we define f_1 and f_2 separately as the low ISR frequency, where $F(f_1) \propto$
 16 $f_1^{-5/3}$ and the high ISR frequency, where again $F(f_2) \propto f_2^{-5/3}$. The two frequencies satisfy the
 17 conditions $f_{KH} < f_1 < f_p$ and $f_2 > f_p$, respectively. The $F_P(f_1)$ is considerably smaller than $F_{KH}(f_1)$, as
 18 illustrated in Fig. 4. Therefore, $F_{KH}(f_1)$ is approximately equal to $F(f_1)$, thereby $F_{KH}(f_1) \propto f_1^{-5/3}$ is
 19 satisfied. This analysis indicates that the TKE dissipation rate calculated through $F(f)$ in the low-
 20 frequency ISR, i.e., labelled as the red line in Fig. 5, represents the cascade dissipation of the shear
 21 turbulence (ϵ_S). Spectral shortcut causes the high frequency ISR for the $F_{KH}(f)$ spectra to coincide
 22 with the ISR for the $F_P(f)$ spectra, as labelled by the dashed black line and the dotted blue line in Fig.
 23 4 (Wilson, 1988), i.e., $F_{KH}(f_2) \propto f_2^{-5/3}$ and $F_P(f_2) \propto f_2^{-5/3}$. Therefore, the sum of them, $F(f_2)$ is also
 24 proportional to $f_2^{-5/3}$, as labelled by the blue line in Fig. 5. The high-frequency ISR for the $F(f)$ spectra
 25 in Fig. 5, thereby, reflects the energy cascading effect in the wake-scale vortices, whose energy
 26 includes both the TKE extracted from the mean flow and part of the TKE transferred from the large
 27 shear-generated eddies.

28 The low-frequency and high-frequency ISRs for the $F(f)$ spectra in the penetration layer are also

1 defined as ISR_{KH} and ISR_P , respectively, as highlighted by the shaded regions in Fig. 5. The ISR_{KH}
 2 and ISR_P values in Fig. 5 agree roughly with the ISR_{KH} for the upper mixing layer and the ISR_P for
 3 the lower canopy zone in Fig. 3, respectively. Because spectral shortcut narrows the ISR_{KH} in the F_{KH}
 4 (f) spectra (Fig. 4), the ISR_{KH} for the F (f) spectra is also narrow for turbulence in the penetration
 5 layer, as shown in Fig. 5.

6 As a result of the spectral shortcut, the dissipation rate ε_S accounts for the difference of the shear
 7 turbulent energy between the one extracted from the mean flow and the one transferred to the wake-
 8 scale turbulence. Therefore, for the TKE budget of the shear turbulence, Eq. (4) can be rearranged as
 9 (Wilson, 1988)

$$10 \quad G_S + T_S - C - \langle \varepsilon_S \rangle = 0 \quad (5)$$

11 where C is the TKE transfer rate caused by spectral shortcut, $\langle \varepsilon_S \rangle$ represents TKE dissipation rate for
 12 the shear turbulence, T_S is TKE transport rate. The TKE transport does not involve energy transfer or
 13 conversion so that the integral along the depth should be zero, i.e., $\int_0^H T_S dz = 0$.

14 4.3 Sub-division of turbulent flow

15 Spectral shortcut affects the KH vortex movement and the vertical flow subdivision because of
 16 the TKE transfer. Now that energy cascading for the shear turbulence has been identified, the flow
 17 subdivision can be studied according to the relative magnitude of the TKE generation rate G_S and the
 18 dissipation term $\langle \varepsilon_S \rangle$. The characteristics of the lower canopy zone is that G_S is smaller than $\langle \varepsilon_S \rangle$,
 19 while in the mixing layer zone G_S becomes larger than $\langle \varepsilon_S \rangle$. The outer zone can easily be
 20 distinguished as the zone where G_S is roughly equal to $\langle \varepsilon_S \rangle$, i.e., the TKE generation and the
 21 dissipation due to shear are in balance (Fig. 6).

22 The subdivision heights of h_p and h_o in different cases are listed in Table 2 (the other terms in
 23 Table 2 will be analyzed in the next section). Comparisons have been made to discuss the influences
 24 of λ , H/h_v and U_m on the vertical development of the KH vortex. It is found that an increase of H/h_v
 25 raises the upper limiting height (h_o) of the mixing layer, while it has little effect on the penetration
 26 height h_p . When $H/h_v = 2$, the upper boundary height h_o does not exist, with G_S being larger than $\langle \varepsilon_S \rangle$
 27 throughout the region above the canopy. The $H/h_v = 2$ represents the condition for the depth-limited

1 flow (Cheng et al., 2012). We therefore conclude that in case of the depth-limited flow, the KH
 2 instability exists, but the vortex structure cannot form due to the inhibition caused by the free surface.
 3 The value of h_o remains nearly constant when $H/h_v \geq 5$, indicating that the upward development of
 4 the KH vortex is almost independent of the submergence. Further, $H/h_v = 5$ also represents the critical
 5 condition which demarcates the **ending** of shallowly-submerged flow (Nepf, 2012a, b).

6 Figure 7a presents the G_S profiles in different H/h_v conditions (with same λ and U_m). The G_S
 7 value decreases with H/h_v around the canopy top, indicating that the small H/h_v intensifies the shear
 8 turbulence. G_S remains vertically constant in the region of $z/h_v > 4.5$ ($z > 27$ cm), and the G_S profile
 9 changes slightly with H/h_v when $H/h_v \geq 5$. The negligible influence of H/h_v on the G_S profile when
 10 $H/h_v \geq 5$ is akin to its influence on the upward vortex development, i.e., the h_o value in Table 2.

11 The lower boundary, h_p increases with λ as vegetation inhibits the penetration of KH vortex
 12 (Table 2). The same has been found in previous studies (Nezu & Sanjou, 2008; Nepf et al., 2007).
 13 The upper boundary height h_o rises with λ when $H/h_v = 3$, and changes little with λ when $H/h_v = 5$,
 14 Table 2. As the large-scale roughness element, an increase of vegetation density λ simultaneously
 15 promotes the shear turbulence generation and dissipation above the canopy (Chen, 2016). The h_o
 16 values in Table 2 suggest that the generation term G_S becomes more prominent as λ increases when
 17 $H/h_v = 3$, with the influence of λ on the G_S profile shown in Fig. 7b. However, the generation and the
 18 dissipation actions caused by λ are offset when $H/h_v = 5$.

19 Neither h_p nor h_o changes with U_m in Table 2. The profiles of non-dimensional G_S varies little
 20 with U_m as seen in Fig. 7c. These results suggest that the high velocity flow does not change the
 21 dominant region of the KH vortex, although it can intensify turbulence.

22 4. 4 Energy transfer by spectral shortcut

23 Spectral shortcut leads to energy transfer, which can be estimated by the TKE budget in the shear
 24 turbulence. Integrating Eq. (5) results in the energy transfer per unit width along the whole depth, CC

$$25 \quad CC = \int_0^H (G_S - \langle \varepsilon_S \rangle) dz \quad (6)$$

26 As the spectral shortcut happens only in the penetration layer, CC divided by the penetration layer
 27 thickness " $h_v - h_p$ " represents the averaged value of the TKE transfer rate C_{ave} , which has been listed
 28 in Table 2. An analysis about C_{ave} values in different cases is conducted to indirectly explore the

1 influences of various factors on the spectral shortcut. Results indicate that: (1) C_{ave} increases with λ
 2 and U_m but decreases with H/h_v ; (2) C_{ave} changes little with H/h_v if $H/h_v \geq 4$. These are similar to the
 3 influences of these factors on the TKE generation rate of the shear turbulence G_S in the penetration
 4 layer, as seen in Fig. 7. A combine of the positive relation between U_m and C_{ave} and the negative
 5 relation between H/h_v and C_{ave} indicates that the influence of the Reynolds number ($U_m \cdot H/\nu$) on
 6 spectral shortcut is complicated and affected by both U_m and H . This happens because the vegetation
 7 drag, rather than the viscous force mainly accounts for flow resistance in the vegetation flow.
 8 Therefore, the expression of ν/H becomes less satisfied to represent the flow resistance in existing
 9 Reynolds number formula.

10 Two terms are defined and then used to investigate the spectral shortcut quantitatively.

$$11 \quad \left\{ \begin{array}{l} \text{shear turbulence: } R_{KH} = \frac{CC}{\int_0^H G_S dz} \times 100\% \\ \text{wake turbulence: } R_W = \frac{CC}{\int_0^{h_v} G_W dz} \times 100\% \end{array} \right. \quad (7).$$

12 where R_{KH} represents the efficiency in the transfer of turbulent energy from the large-scale, shear
 13 turbulence to the secondary turbulence, R_W represents the ratio of the secondary turbulent energy to
 14 the wake turbulent energy.

15 R_{KH} varies from 58% to 71% as can be seen in Table 2, which implies that a significant portion
 16 of TKE of the shear turbulence is consumed by energy transfer. The R_{KH} is affected by the value of
 17 U_c , and R_{KH} would range from 37% to 57% if $U_c = U$ is selected and would vary from 69% to 78% if
 18 $U_c = 2U$. The value of R_W is larger than 1 in some of the cases, especially in conditions with $\lambda = 1.44$
 19 (see Table 2). This phenomenon suggests that the main contributor to the wake-scale turbulence is the
 20 energy transferred from the shear turbulence (i.e., the secondary turbulent energy), rather than the one
 21 extracted from the mean flow (i.e., the wake turbulent energy).

22 In the terrestrial canopy flow (Wilson, 1988), C was calculated as:

$$23 \quad C = \frac{1}{2} C_d \frac{\lambda}{h_v} \langle U \rangle \cdot \left[2 \langle u'^2 \rangle + \langle v'^2 \rangle + \langle w'^2 \rangle \right] \quad (8),$$

24 The universality of Eq. (8) can be judged by comparing the integral CI with CC in Table 2, where

$$CI = \int_0^{h_v} \frac{1}{2} C_d \frac{\lambda}{h_v} \langle U \rangle [2\langle u'^2 \rangle + \langle v'^2 \rangle + \langle w'^2 \rangle] dz \quad (9).$$

The value of CC approximates to that of CI only in A-2-20, B-2-20, D-2-20 and E-2-20 conditions. The ratio of the channel width to water depth B/H is equal to 5 for these cases, where the sidewall effect is weak and the channel can be treated as wide (Nezu & Nakagawa, 1993). Therefore, Eq. (8) may be applicable only in wide and shallow flows.

5. Conclusions

The turbulent velocity measurement and spectrum analysis were conducted based on the experiments in an open channel with submerged rigid vegetation. The purpose of this investigation was to understand the spectral shortcut characteristics between the KH and wake-scale vortices. The results have been discussed in terms of the spectral distribution, flow subdivision and energy transfer. The main findings of this investigation are summarized as follows.

1. The spectral distribution may exhibit one of the three different forms depending on the elevations. The lower canopy zone has a high-frequency ISR, the upper mixing layer has a low-frequency ISR, whereas the intermediate penetration layer contains both high- and low-frequency ISRs.

2. The existence of the dual ISRs in the turbulent spectra is evident in the penetration layer, which is caused by the spectral shortcut. 58-71% of the shear turbulent energy is transferred from the large-scale shear turbulence to the wake-scale turbulence over the depth.

3. Dense vegetation promotes the upward movement of the KH vortex when the submergence H/h_v is 3. However, vegetation density does not affect the upward development of the vortex in a shallowly submerged flow with $H/h_v = 5$.

4. The transferred TKE plays an important role in driving the wake-scale turbulence. The TKE transfer rate increases with the increase of λ and U_m and a decrease of H/h_v .

Although the TKE dissipation rate ε was estimated in this study based on the Kolmogorov's -5/3 power law, a more rigorous way to calculate ε will be needed in more complicated flow conditions. Many additional features, such as the influence of the sidewalls, the vortex development over flexible vegetation, the uneven bed topography and channel morphology need in-depth study in the future.

1 Some efforts should be paid to seek for a better Reynolds number expression that represents the ratio
2 between the inertial force and flow resistance in vegetation flow, and the influence of the Reynolds
3 number on turbulent motion and the spectral shortcut should also be explored.

4 **Acknowledgement**

5 This work was partly supported by the National Natural Science Foundation of China [grant
6 numbers 51579079, 51979084, 51239003]; the 111 Project [grant number B17015]; and China
7 Scholarship Council project [grant number 201806715026]. We also thank Professor Bidya Sagar
8 Pani and [Professor Saiyu Yuan](#) for their help in revising this work.

9 **References**

- 10 Blevins, R. D., 2006. Flow-induced vibration. Krieger Publishing Company, Malabar.
- 11 Bouteiller, C. L., Venditti, J. G., 2014. Vegetation- driven morphodynamic adjustments of a sand bed.
12 *Geophys. Res. Lett.* 41(11), 3876-3883. <https://doi.org/10.1002/2014GL060155>
- 13 Bouteiller, C. L., Venditti, J. G., 2015. Sediment transport and shear stress partitioning in a vegetated
14 flow. *Water Resour. Res.* 51(4), 2901-2922. <https://doi.org/10.1002/2014WR015825>
- 15 Chen, B., 2011. Investigation of near-wake flow characteristics of two circular cylinders close to a
16 wall based on PIV technology (Ph.D. thesis). Huazhong University of Science & Technology, Wuhan.
- 17 Chen, Z. G., Guo, P., 2013. Numerical Simulation of aerodynamic noise induced by flow around a
18 circular cylinder. *Technical Acoustics.* 32(4), 65-68. (in Chinese)
- 19 Chen, Y., 2016. Experimental study on turbulence characteristic height and turbulence energy budget
20 in open channel flows with vegetation (Master thesis). Hohai University, Nanjing.
- 21 Cheng, N. S., Nguyen, H. T., Tan, S. K., Shao, S. D., 2012. Scaling of velocity profiles for depth-
22 limited open channel flows over simulated rigid vegetation. *J. Hydraul. Eng.* 138(8), 673-683.
23 [https://doi.org/10.1061/\(ASCE\)HY.1943-7900.0000562](https://doi.org/10.1061/(ASCE)HY.1943-7900.0000562)
- 24 Choi, S. U., Kang, H., 2016. Characteristics of mean flow and turbulence statistics of depth-limited
25 flows with submerged vegetation in a rectangular open-channel. *J. Hydraul. Res.* 54(5), 527-540.
26 <https://doi.org/10.1080/00221686.2016.1168882>
- 27 Finnigan, J., 2000. Turbulence in plant canopies. *Annu. Rev. Fluid Mec.* 32, 519-571.

1 <https://doi.org/10.1146/annurev.fluid.32.1.519>

2 Ghisalberti, M., Nepf, H. M., 2002. Mixing layers and coherent structures in vegetated aquatic flows.
3 J. Geophys. Res. 107(C2). <https://doi.org/10.1029/2001JC000871>

4 Ghisalberti, M., Nepf, H. M., 2006. The structure of the shear layer in flows over rigid and flexible
5 canopies. Environ. Fluid Mech. 6(3), 277-301. <https://doi.org/10.1007/s10652-006-0002-4>

6 Hout, R. Van, Zhu, W., Luznik, L., Katz, J., Kleissl, J., Parlange, M. B., 2007. PIV measurements in
7 the atmospheric boundary layer within and above a mature corn canopy. Part I: statistics and energy
8 flux. J. Atmos. Sci. 64(8), 2805-2824. <https://doi.org/10.1175/JAS3989.1>

9 Huai, W. X., Zeng, Y. H., Xu, Z. G., Yang, Z. H., 2009. Three-layer model for vertical velocity
10 distribution in open channel flow with submerged rigid vegetation. Adv. Water Resour. 32(4), 487-
11 492. <https://doi.org/10.1016/j.advwatres.2008.11.014>

12 Kemp, J. L., Harper, D. M. & Crosa, G. A., 2000. The habitat- scale ecohydraulics of rivers. Ecol.
13 Eng. 16(1), 17-29. [http://doi.org/10.1016/S0925-8574\(00\)00073-2](http://doi.org/10.1016/S0925-8574(00)00073-2)

14 King, A. T., Tinoco, R. O., Cowen, E. A., 2012. A k - ϵ turbulence model based on the scales of vertical
15 shear and stem wakes valid for emergent and submerged vegetated flows. J. Fluid Mech. 701, 1-39.
16 <https://doi.org/10.1017/jfm.2013.113>

17 Liu, D., Diplas, P., Hodges, C. C., Fairbanks, J.D., 2010. Hydrodynamics of flow through double
18 layer rigid vegetation. Geomorphology. 116 (3-4), 286- 296.
19 <http://dx.doi.org/10.1016/j.geomorph.2009.11.024>

20 Liu, S. H., Liu, H. P., Xu, M., Leclerc, M. Y., Zhu, T. Y., Jin, C. J., Hong Z. X., Li, J., & Liu, H. Z.,
21 2001. Turbulence spectra and dissipation rates above and within a forest canopy. Bound- lay. Meteorol.
22 98(1), 83-102. <https://doi.org/10.1023/A:1018715812229>

23 Mandel, T.L., Rosenzweig I., Chung, H., Ouellette N.T., Koseff, J.R., 2017. Characterizing free-
24 surface expressions of flow instabilities by tracking submerged features. Exp. Fluids. 58, 153.
25 <https://doi.org/10.1007/s00348-017-2435-6>.

26 Monin, A.S., Yaglom, A.M., 1975. Statistical fluid mechanics: mechanics of turbulence, vol. II. MIT
27 Press, Boston.

28 Nepf, H. M., 1999. Drag, turbulence, and diffusion in flow through emergent vegetation. Water
29 Resour. Res. 35(2), 479-489. <https://doi.org/10.1029/1998WR900069>

1 Nepf, H. M., Vivoni, E. R., 2000. Flow structure in depth-limited, vegetated flow. *J. Geophys. Res.*
2 105(C12), 28547-28557. <https://doi.org/10.1029/2000JC900145>

3 Nepf, H., Ghisalberti, M., White, B., Murphy, E., 2007. Retention time and dispersion associated with
4 submerged aquatic canopies. *Water Resour. Res.* 43, W04422.
5 <https://doi.org/10.1029/2006WR005362>

6 Nepf, H., Ghisalberti, M., 2008. Flow and transport in channels with submerged vegetation. *Acta*
7 *Geophys.* 56(3), 753-777. <https://doi.org/10.2478/s11600-008-0017-y>

8 Nepf, H. M., 2012a. Flow and transport in regions with aquatic vegetation. *Annu. Rev. Fluid Mec.*
9 44, 123-142. <https://doi.org/10.1146/annurev-fluid-120710-101048>

10 Nepf, H. M., 2012b. Hydrodynamics of vegetated channels. *J. Hydraul. Res.* 50(3), 262-279.
11 <http://dx.doi.org/10.1080/00221686.2012.696559>

12 Nezu, I., Nakagawa, H., 1993. *Turbulence in open-channel flows*. A. A. Balkema, Rotterdam.

13 Nezu, I., Sanjou, M., Okamoto, T., 2006. Turbulent structure and dispersive properties in vegetated
14 canopy open-channel flows. Paper presented at River Flows 2006, Balkema.

15 Nezu, I., Sanjou, M., 2008. Turbulence structure and coherent motion in vegetated canopy open-
16 channel flows. *J. Hydro-environ. Res.* 2(2), 62-90. <https://doi.org/10.1016/j.jher.2008.05.003>

17 Okamoto, T., Nezu, I., 2013. Spatial evolution of coherent motions in finite- length vegetation patch
18 flow. *Environ. Fluid Mech.* 13(5), 417-434. <https://doi.org/10.1007/s10652-013-9275-6>

19 Perignon, M. C., Tucker, G. E., Griffin, E. R., Friedman, J. M., 2013. Effects of riparian vegetation
20 on topographic change during a large flood event, Rio Puerco, New Mexico, USA. *J. Geophys. Res.*
21 - *Earth.* 118(3), 1193-1209. <https://doi.org/10.1002/jgrf.20073>

22 Poggi, D., Porporato, A., Ridolfi, L., Albertson, J. D., Katul, G. G., 2004. The effect of vegetation
23 density on canopy sub-layer turbulence. *Bound- lay. Meteorol.* 111(3), 565-587.
24 <https://doi.org/10.1023/B:BOUN.0000016576.05621.73>

25 Raupach, M. R., Shaw, R. H., 1982. Averaging procedures for flow within vegetation canopies.
26 *Bound- lay. Meteorol.* 22(1), 79-90. <https://doi.org/10.1007/BF00128057>

27 Raupach, M. R., Finnigan, J. J., Brunet, Y., 1996. Coherent eddies and turbulence in vegetation
28 canopies: the mixing analogy. *Bound- lay. Meteorol.* 78, 381-352.

1 https://doi.org/10.1007/978-94-017-0944-6_15

2 Ricardo, A. M., Koll, K., Franca, M. J., Schleiss, A.J., Ferreira R. M. L., 2014. The terms of turbulent
3 kinetic energy budget within random arrays of emergent cylinders. *Water Resour. Res.* 50, 4131-4148.
4 <https://doi.org/10.1002/2013WR014596>

5 Tang, H. W., Tian, Z. J., Yan, J., Yuan, S. Y., 2014. Determining drag coefficients and their application
6 in modelling of turbulent flow with submerged vegetation. *Adv. Water Resour.* 69, 134-145.
7 <https://doi.org/10.1016/j.advwatres.2014.04.006>

8 Wallace, S., Luketina, D., Cox, R., 1998. Large scale turbulence in seagrass canopies. Paper presented
9 at 13th Australasian Fluid Mechanics Conference, Melbourne.

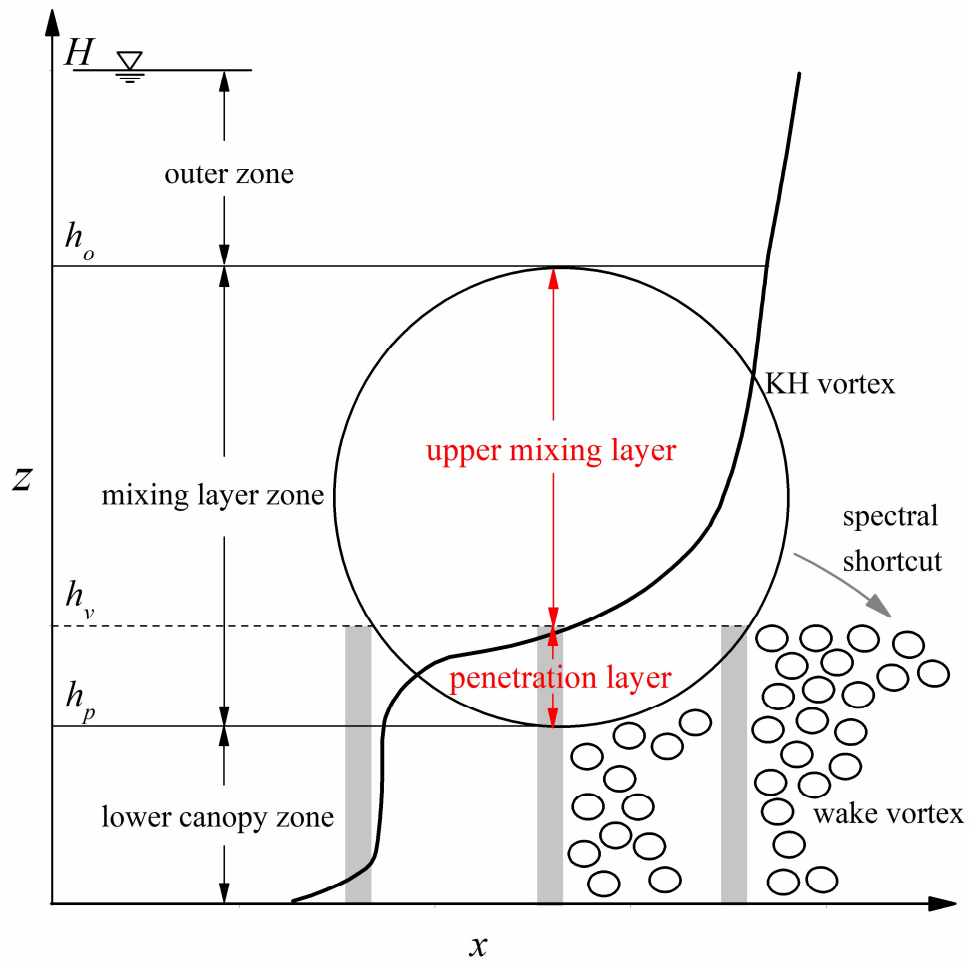
10 Wilson, J.D., 1988. A second-order closure model for flow through vegetation. *Bound- lay. Meteorol.*
11 42, 371-392.

12 Yang, W. J., Choi, S. U., 2010. A two-layer approach for depth-limited open-channel flows with
13 submerged vegetation. *J. Hydraul. Res.* 48(4), 466-475.
14 <https://doi.org/10.1080/00221686.2010.491649>

15 Yuan, S. Y., Tang, H. W., Xiao, Y., Qiu, X. H., Zhang, H. M., Yu, D. D., 2016. Turbulent flow structure
16 at a 90-degree open channel confluence: Accounting for the distortion of the shear layer. *Journal of*
17 *Hydro- environment Research.* 12, 130- 147. <http://dx.doi.org/10.1016/j.jher.2016.05.006>

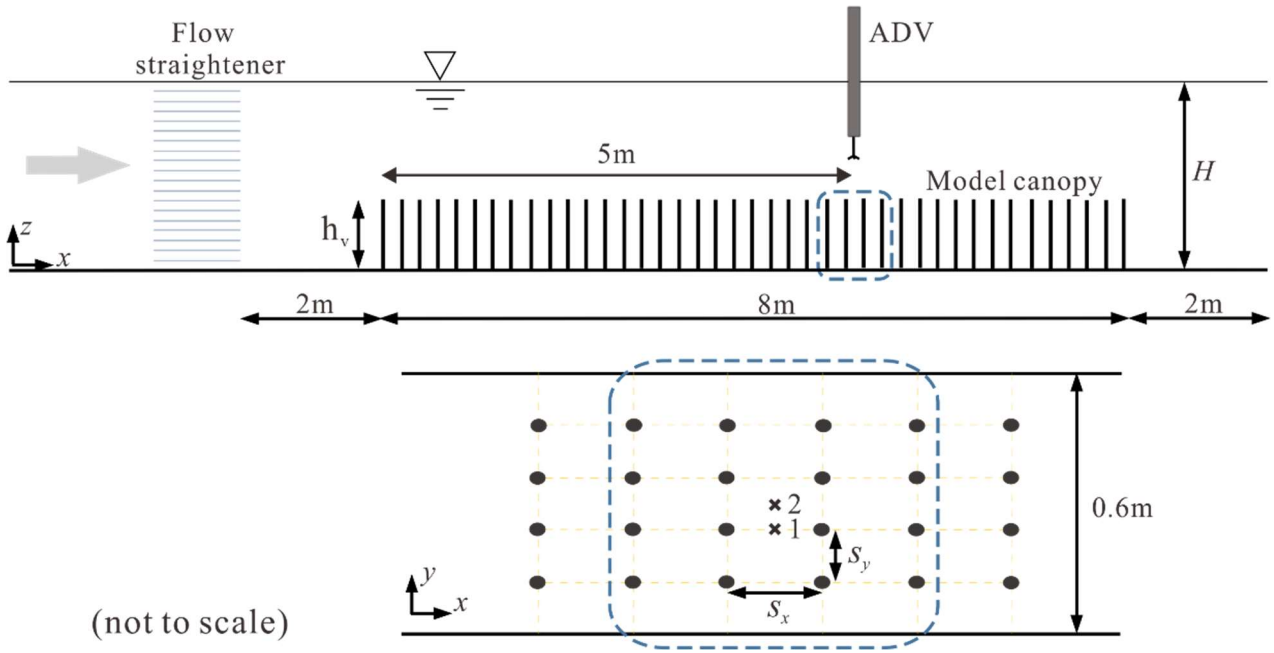
18 Zhao, H. Q., Yan, J., Yuan, S. Y., Liu, J. F., Zheng, J. Y., 2019. Effects of submerged vegetation density
19 on turbulent flow characteristics in an open channel. *Water- sui.* 11(10), 2154.
20 <https://doi.org/10.3390/w11102154>

21 Zong, L. J., Nepf, H., 2010. Flow and deposition in and around a finite patch of vegetation.
22 *Geomorphology.* 116(3-4), 363-372. <https://doi.org/10.1016/j.geomorph.2009.11.020>



1
2

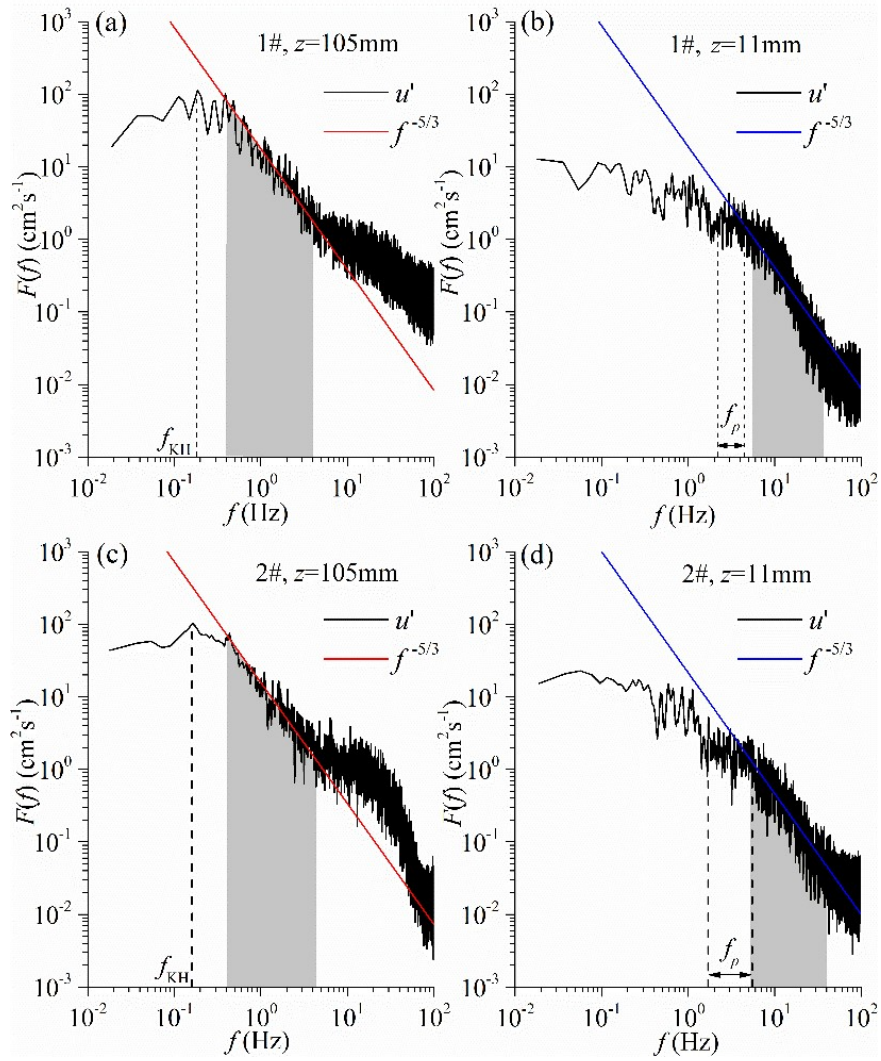
Fig. 1. Schematic description of vortical structure in submerged vegetated flow.



(not to scale)

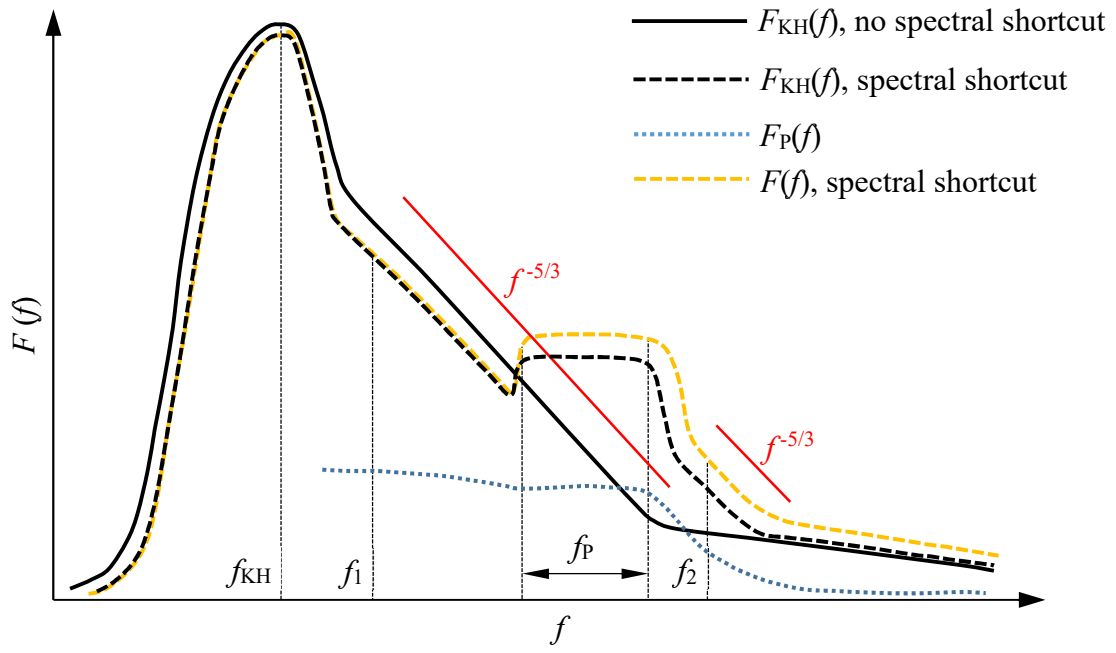
1
2
3

Fig. 2. A schematic of the experimental setup: flume system, vegetation layer, and measurement locations (Zhao et al., 2019).



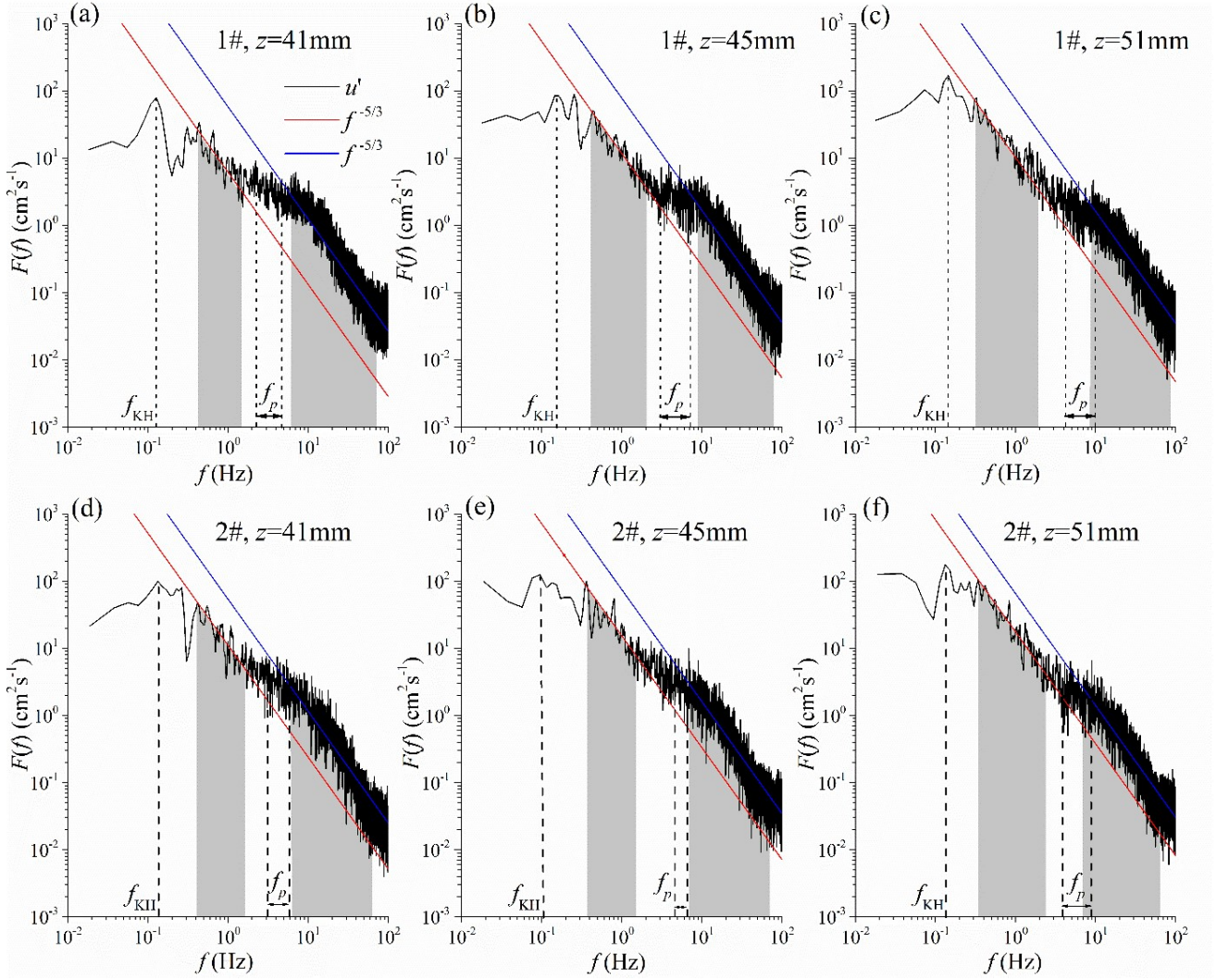
1
2
3

Fig. 3. Spectral distributions at different heights of location 1 and 2 with the ISR in shaded region (Case B-3-30).



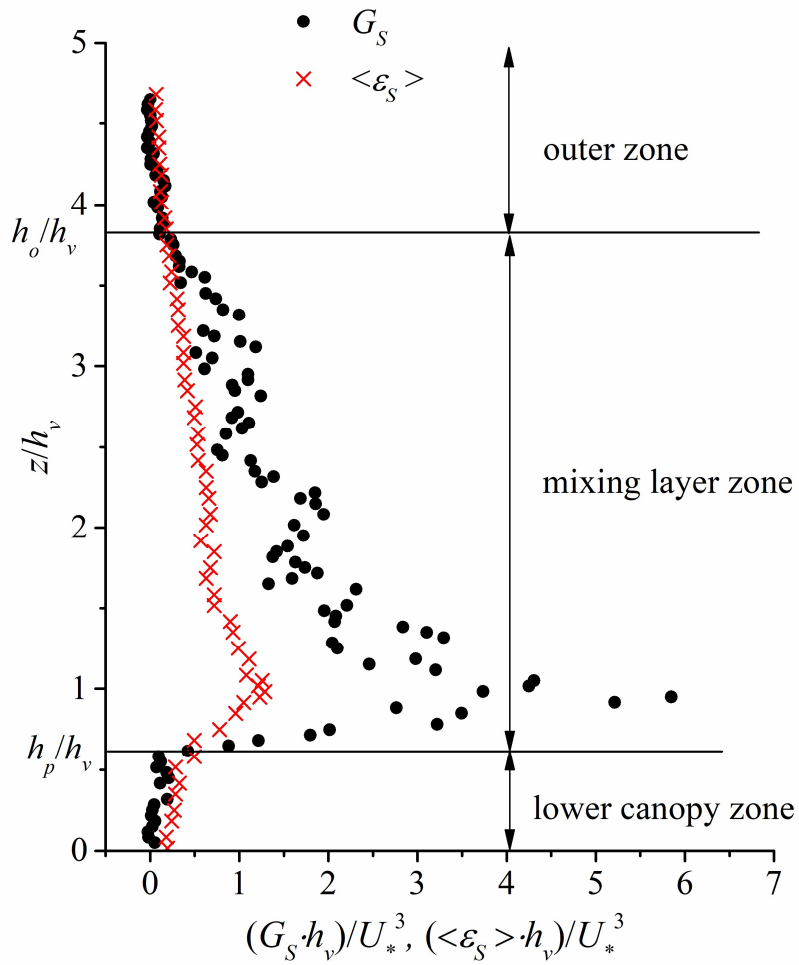
1
2
3

Fig. 4. Schematic diagram (log-log) illustrating the influence of spectral shortcut on turbulent spectra.



1

2 **Fig. 5.** The phenomenon of dual ISRs for turbulent spectra in the penetration layer (Case B-3-30).



1

2 **Fig. 6.** G_S and $\langle \varepsilon_S \rangle$ profiles and flow subdivision for Case B-5-30 with $U_* = \sqrt{gS(H - h_v)}$.

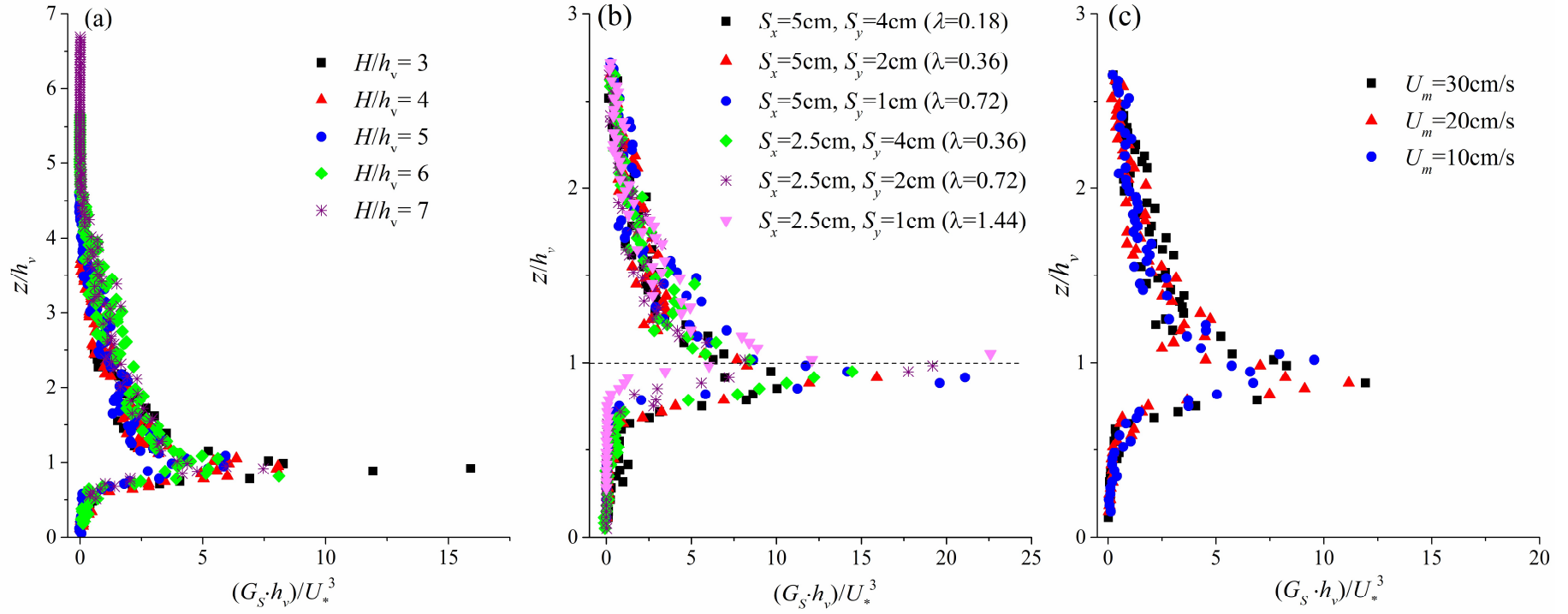


Fig. 7. G_s profiles in different (a) H/h_v , (b) S_x, S_y and (c) U_m conditions.

1
2

Table 1. Experimental conditions

Case	S_x (cm)	S_y (cm)	λ	H (cm)	H/h_v	Q (L s ⁻¹)	U_m (cm s ⁻¹)	S ‰
A-2-20	5	4	0.18	12	2	14.35	19.93	1.92
A-3-30	5	4	0.18	18	3	32.40	30.00	1.58
A-5-30	5	4	0.18	30	5	54.03	30.02	0.83
B-2-20	5	2	0.36	12	2	14.34	19.92	2.92
B-3-30	5	2	0.36	18	3	32.40	30.00	2.33
B-3-20	5	2	0.36	18	3	21.68	20.07	1.21
B-3-10	5	2	0.36	18	3	10.77	9.97	0.29
B-4-30	5	2	0.36	24	4	43.28	30.06	1.33
B-5-30	5	2	0.36	30	5	53.97	29.98	0.92
B-6-30	5	2	0.36	36	6	64.64	29.93	0.58
B-7-30	5	2	0.36	42	7	75.50	29.96	0.5
C-3-30	5	1	0.72	18	3	32.40	30.00	3.08
C-5-30	5	1	0.72	30	5	53.96	29.98	1
D-2-20	2.5	4	0.36	12	2	14.42	20.03	1.96
D-3-30	2.5	4	0.36	18	3	32.38	29.98	1.75
D-5-30	2.5	4	0.36	30	5	53.92	29.96	0.75
E-2-20	2.5	2	0.72	12	2	14.41	20.01	3.58
E-3-30	2.5	2	0.72	18	3	32.47	30.06	2.83
E-5-30	2.5	2	0.72	30	5	54.00	30.00	0.98
F-3-30	2.5	1	1.44	18	3	32.48	30.07	3.75
F-5-30	2.5	1	1.44	30	5	53.91	29.95	1.17

- 2 Notes: (1) flow discharge Q was recorded every 2 h in the experiment, and the average was reported in the table and
3 (2) each run is assigned a code. For example, case- A-2-20 stands for run A ($S_x = 5$ and $S_y = 4$ cm) with $H/h_v = 2$ and
4 $U_m = 20$ cm s⁻¹ (rounded).

1

Table 2. Subdivision heights and energy transfer in different cases.

Case	h_p (mm)	h_o (mm)	C_{ave} (cm ² s ⁻³)	CC (cm ³ s ⁻³)	CI (cm ³ s ⁻³)	R_{KH} (%)	R_w (%)
A-2-20	31	—	32.45	94.1	80.02	69.84	28.63
A-3-30	37	125	135.91	312.6	274.69	63.85	55.08
A-5-30	35	211	108.36	270.9	133.99	62	118.49
B-2-20	41	—	130.84	248.6	289.33	71.45	47.54
B-3-30	39	141	304.86	640.2	491.85	69.15	112.51
B-3-20	41	137	96.05	182.5	123.93	69.01	106.24
B-3-10	41	141	10.79	20.5	18.99	65.36	92.33
B-4-30	35	199	162.92	407.3	334.01	59.45	104.99
B-5-30	39	227	142.95	300.2	194.69	57.59	109.32
B-6-30	41	235	154.89	294.3	151.51	61.06	178.62
B-7-30	39	231	*	*	*	*	*
C-3-30	47	145	775.38	1008	470.51	63.68	312.88
C-5-30	45	215	296.07	444.1	149.3	63.16	555.55
D-2-20	31	—	38.28	111	110.71	64.51	26.51
D-3-30	45	125	289.20	433.8	258.27	69.45	77.71
D-5-30	41	211	138.68	263.5	109.4	62.49	124.28
E-2-20	43	—	129.68	220.45	287.9	70.46	45.57
E-3-30	45	135	416.53	624.8	435.49	59.9	108.60
E-5-30	47	219	294.00	382.2	218.67	58.51	230.58
F-3-30	55	151	2030.00	1015	327.01	64.46	1194.14
F-5-30	55	209	925.20	462.6	142.73	60.45	1087.27

2 Notes: (1) — indicates that the subdivision height where TKE balance changes is not available; (2) * indicates that
3 the value is not available because the flow field for $z < 3$ cm cannot be measured and an integral along the water
4 depth is invalid and (3) values in the table are calculated by piecewise linear interpolation.

5